Journal of Pharmaceutical and Biomedical Analysis 179 (2020) 113017

Contents lists available at ScienceDirect

Journal of Pharmaceutical and Biomedical Analysis

journal homepage: www.elsevier.com/locate/jpba

Advanced nanomedicine characterization by DLS and AF4-UV-MALS: Application to a HIV nanovaccine

Marlène Klein[a,*], Mathieu Menta[a], Tamara G. Dacoba[b,c], José Crecente-Campo[b,c], María J. Alonso[b,c], Damien Dupin[e], Iraida Loinaz[e], Bruno Grassl[d], Fabienne Séby[a]

[a] Ultra Trace Analyses Aquitaine (UT2A/ADERA), Technopôle Hélioparc Pau-Pyrénées, 2 Avenue du Président Angot, PAU Cedex 9, 64053, France
[b] Center for Research in Molecular Medicine and Chronic Diseases (CIMUS), Campus Vida, Universidade de Santiago de Compostela, Santiago de Compostela, 15782, Spain
[c] Department of Pharmacology, Pharmacy and Pharmaceutical Technology, School of Pharmacy, Campus Vida, Universidade de Santiago de Compostela, Santiago de Compostela, 15782, Spain
[d] Institut des Sciences Analytiques et de Physico-chimie pour l'Environnement et les Matériaux (IPREM), UMR 5254, CNRS-Université de Pau et des Pays de l'Adour, Technopôle Hélioparc Pau-Pyrénées, 2 Avenue du Président Angot, PAU Cedex 9, 64053, France
[e] CIDETEC, Basque Research and Technology Alliance (BRTA), P[º] Miramón, 196, Donostia-San Sebastián, 20014, Spain

ARTICLE INFO

Article history:
Received 6 September 2019
Received in revised form 31 October 2019
Accepted 27 November 2019
Available online 30 November 2019

Keywords:
Polymeric nanoparticles
Nanovaccine
Asymmetrical flow field-flow fractionation
Dynamic light scattering

ABSTRACT

Nanoformulations are complex systems where physicochemical properties determine their therapeutic efficacy and safety. In the case of nanovaccines, particle size and shape play a crucial role on the immune response generated. Furthermore, the antigen's integrity is also a key aspect to control when producing a nanovaccine. The determination of all those physicochemical properties is still an analytical challenge and the lack of well-established methods hinders the access of new therapeutics to the market. In this work, robust methods for the characterization of a novel HIV nanoparticle-based vaccine produced in good manufacturing practice (GMPs)-like environment were developed. With slightly polydisperse particles (< 0.2) close to 180 nm of size, batch-mode Dynamic Light Scattering (DLS) was validated to be used as a quality control technique in the pilot production plant. In addition, a high size resolution method using Asymmetrical Flow Field Flow Fractionation (AF4) demonstrated its ability to determine not only size and size distribution but also shape modification across the size and accurate quantification of the free active ingredient. Results showed a monomodal distribution of particles from 60 to 700 nm, most of them (> 90%) with size lower than 250 nm, consistent with more traditional techniques, and revealed a slight change in the structure of the particles induced by the presence of the antigen. Finally, a batch to batch variability lower than 20% was obtained by both DLS and AF4 methods indicating that preparation method was highly reproducible.

1. Introduction

In the last decades, the development of polymeric nanoparticles (NPs) as carriers for vaccine delivery has exponentially grown [1–4]. With a size similar to a virus, NPs facilitate the transport of antigens through biological barriers to reach the targeted immune cells. Several works have demonstrated the capacity of NPs to enhance antigen bioavailability and to modulate the generated immune response [1,2]. Besides, due to their interesting properties (bioavailability, biocompatibility, biodegradability, low price, etc.), nanoparticles made of natural polymers have attracted high interest [3,4]. Among all these polymers, chitosan is particularly used due to its mucoadhesive properties for mucosal administration [3–5]. In 1997, Calvo et al. developed hydrophilic chitosan NPs, formed by ionic gelation, capable of harboring protein antigens [6,7]. Since then, the use of chitosan NPs for vaccine delivery has been extensively studied but, despite these efforts, no chitosan-based vaccine has reached the market yet [8]. As described by the Food and Drug Administration (FDA) and the European Commission [9,10], the lack of well-assessed robust routine analytical methods for quality control hinders further development and delays the regulatory acceptance of nanomedicines.

Preclinical physicochemical characterization of nanoformulations is essential to fully understand their biodistribution, pharmacokinetic and safety profiles [11]. Size is one of the key parameters for nanovaccine efficacy, determining the cellular

* Corresponding author.
E-mail address: marlene.klein@univ-pau.fr (M. Klein).

https://doi.org/10.1016/j.jpba.2019.113017
0731-7085/

uptake mechanism and influencing the immunogenicity [1,2,12]. Therefore, it is crucial to accurately determine the overall range of NPs size within the formulation [13]. To reach this information, it is recommended to work with complementary methods in order to obtain a realistic and complete knowledge of the nanosystem [13–15]. Up to now, the techniques referenced in international standard organization (ISO) guidelines and recognized by health agencies are electron microscopy (EM), dynamic light scattering (DLS), small angle X-ray scattering (SAXS), atomic force microscopy (AFM), and nanoparticle tracking analysis (NTA) [16,17].

DLS is the most commonly used technique for size distribution determination of nanocarriers because of its simplicity of use and its attractive price. In the case of a homogeneous single size population, DLS is sufficient to achieve accurate size determination [18,19]. Kato et al. [20] demonstrated that polydispersity (PDI) values obtained by DLS are also useful for representing the relative difference in the size distribution for particles with a wider size distribution. However, in the case of complex and polydisperse nanoformulations, DLS can lead to confusing and misleading results because of its poor specificity and resolution. [21]. Its use according to the ISO standard [22], assuming a monomodal and gaussian distribution, is thus often far from reality [14].

Therefore, to increase the accuracy of size analysis and to obtain more detailed information on other critical sample characteristics, such as shape or sample composition, the implementation of more advanced techniques is required [15]. Hyphenation of light scattering detectors with size-based separation can be an interesting approach. Size exclusion chromatography (SEC) is a valuable technique for size-based NPs separation in complex samples [23], but its limited size range (generally < 100 nm) and interactions of NPs with the stationary phase are important drawbacks [24,25]. Asymmetrical Flow Field Flow Fractionation (AF4) has the advantage of separating macromolecules or particles over a wide size range (from 1 to 1000 nm) and is classified as a soft fractionation technique. Reviewed in many publications [26–30], AF4 was recently standardized by ISO [31] and recognized by the medicine regulatory agencies [16]. According to the associated detector, AF4 allows the acquisition of key parameters, which makes it an adequate technique for analysis of such complex samples. AF4 has already been applied to several nanomedicines including liposomes, lipid NPs, polymeric NPs, virus like particles (VLP) and metallic particles [28]. McEvoy et al. developed an AF4 - Multi-Angle Light Scattering (MALS) method for size analysis and quantification of VLP populations, showing a good correlation with NTA and microscopy techniques [32]. Moreover, with the use of concentration detectors, drug loading and particle stability studies of liposomes have been performed [33]. However, to our knowledge, its use as a unique and complete analytical method for nanovaccine characterization has not been reported yet.

The purpose of this work was to develop robust methods for the physicochemical characterization of a novel HIV nanovaccine under preclinical studies. The synthesis of nanovaccine is based on ionic interactions between antigen and biopolymers (chitosan and dextran sulfate). During the formulation development, the vaccine was basically characterized in terms of size by DLS and then transferred from the laboratory to a pilot plant operating in a good manufacturing practices (GMPs)-like environment for the production of small batches. The improvement of the analytical characterization presented herein was performed in parallel to this scaling-up. As highly recommended by many authors [14,15], several characterization methods were combined in order to achieve accurate size determination and reliable results. Batch-mode DLS analysis was validated in accordance to ICH guidelines [34] in order to be used as a quality control technique at the NPs production plant. In combination with DLS, AF4 with multidetection system (MALS and UV) was also optimized for the determination of NPs size, size distribution, shape, as well as for antigen quantification. Results were then compared to more traditional analytical techniques (DLS, NTA, EM, and SEC-UV). Once analytical performances were obtained, AF4 and DLS were applied to the analysis of several batches for process variability evaluation.

2. Materials and methods

2.1. Instrumentation

Batch-mode Dynamic Light Scattering (DLS) analyses were performed using a VASCO-2 particle size analyzer (Cordouan Technology, France) in combination with the software nanoQ v 6.2.2. DLS is equipped with a 65 mW laser (657 nm wavelength) located at 135°.

UV-Visible spectra of reconstituted nanoformulation was acquired from 400 nm to 800 nm using a UV-2401 (PC) (Shimadzu, Japan).

The instrumentation used for size separation of NPs consisted of an Agilent 1260series autosampler and a HPLC pump (Agilent Technologies, USA) with an Asymmetrical Flow Field Flow Fractionation (AF4) Eclipse® flow control module (Wyatt Technology, USA) and a long separation channel (275 mm length). AF4 membranes and spacer were purchased from Wyatt Technology. An online PVDF filter with 0.1 μm pore size (Millipore, USA) was added between the pump and the Eclipse flow module. Mobile phases were filtered before use at 0.1 μm with a cellulose nitrate filter (Whatman, Germany). The detection chain contained a UV–vis detector operating at 214 nm in order to obtain an optimal signal for antigen analysis (VWD 1200 series, Agilent Technologies) and a Multi-Angle Light Scattering (MALS) detector of 18 angles operating at 662 nm (laser wavelength given by the provider) (DAWN HELEOS II, Wyatt Technology). Data from the different detectors were collected and treated with the Astra v 6.1.2. software (Wyatt Technology) that includes the band broadening correction.

Z-potential measurements were performed with a zetasizer Wallis (Cordouan Technology, France) used in combination with the software zetaQ v 1.7. Samples were prepared in SDS 0.1% (w/v), used as a carrier for AF4 measurement.

Microscopy images were obtained with a field emission scanning electron microscopy (FESEM) (Zeiss Gemini Ultra Plus, Germany). Scanning Transmission Electron Microscopy (STEM) and immersion lens (InLens) detectors were used for sample imaging. Image J was used for data treatment [35].

Nanoparticle tracking analysis was performed with a NanoSight NS3000 (Malvern Instruments, United Kingdom) with the software Nanosight NTA v3.3 for data treatment.

Antigen content was determined with an Agilent 1260series autosampler and a HPLC pump (Agilent Technologies, USA) equipped with a Superdex peptide 10/300 G L column (GE Healthcare Europe, Switzerland) hyphenated to an UV–vis detector operating at 214 nm (VWD 1200 series, Agilent Technologies).

2.2. Chemicals

For AF4 size calibration and quality control purposes, polystyrene nanosphere suspensions (PS) NIST traceable with a diameter of 23 ± 2 nm (PS20); 46 ± 2 nm (PS50); 100 ± 3 nm (PS100) and 203 ± 5 nm (PS200) stated by Transmission Electron Miscroscopy (TEM) were used (Thermo Fisher Scientific, USA).

Sodium chloride (BioXtra ≥ 98.5%), sodium dihydrogenophosphate monohydrate (ACS reagent ≥ 98.0%), sodium phosphate (BioXtra ≥ 99.0%) and sodium dodecyl sulfate (SDS, Reagent Plus ≥ 98.5%), used as carriers for SEC and AF4 analysis were purchased from Sigma (USA). Ultrapure water (18.2 MΩ.cm, TOC < 10 ppb)

used for sample dispersion and AF4 mobile phase preparation was obtained from a milli-Q instrument equipped with 0.1 μm filter cartridge (Millipore, USA).

Bovine Serum Albumin (monomer ≥ 97%) and toluene (HPLC Plus ≥ 99.9%) used for MALS normalization and calibration, respectively, were purchased from Sigma (USA). Sodium hydroxide (ACS reagent ≥ 98.0%) used for NPs disruption and glycerol (ACS reagent ≥ 99.5%) used for centrifugation were also purchased from Sigma (USA).

Polymeric nanoparticles were prepared by electrostatic interactions between chitosan hydrochloride (GMP grade, Mw 30−400 kDa, Heppe Medical HMC+, Germany) and dextran sulfate (pharmaceutical grade, Mw 8 kDa, Dextran Products limited, Canada). The loaded peptide antigen PCS5 – 68-1, patent number CA2012050220 [36], has a molecular weight of 2.28 kDa and was purchased from GenScript (USA). Trehalose dihydrate of pharmaceutical grade used for freeze drying was purchased from Pfansthiel (Switzerland).

2.3. Nanoformulation synthesis and specifications

The formulation was designed to be used for intranasal administration. Briefly, the synthesis of nanoparticles was based on the ionic complexation of positively-charged components (peptide antigen and chitosan) with the anionic dextran sulfate, as described in previous studies [37,38]. The optimal mass ratio of the three components was 0.4:1:3, respectively, with a final peptide concentration of 0.133 mg/mL. Each batch was divided in aliquots of 900 μL. In each aliquot, 180 μL of trehalose 45% wt in water were added as cryoprotectant for the freeze-drying process. Nine batches of antigen-loaded nanoparticles were produced (batches L1 to L9). Four batches of control nanoparticles (batch C1 to C4) not containing the antigen were also prepared following the same procedure to study the interactions of peptide with the NPs and evaluate its effect on the NPs behavior. Product specifications in terms of size and size distribution of loaded NPs using batch-mode DLS measurement were previously defined (Table 2). They are based on the appropriate characteristics to reach the target tissue from the mucosal route [2].

2.4. Sample preparation for NPs characterization

Sample preparation for analysis was similar to the preparation expected for patient administration. Freeze dried formulations were reconstituted in ultrapure water at 6.4% wt and vortexed for 20 s. Samples were then directly analyzed or kept at 4 °C until analysis. Concentration of the components in the reconstituted formulation were 0.7031 mg/mL for dextran sulfate; 0.2345 mg/mL for chitosan hydrochloride; 0.100 mg/mL for the peptide antigen and 67.5 mg/mL for trehalose.

2.5. Analytical procedures for NPs characterization

The analytical procedures applied for the nanoformulation characterization are presented in Fig. 1. Besides all those techniques, Z-potential analysis was performed to compare the surface charge of NPs with that of PS standards during AF4 separation. EM, NTA and SEC-UV techniques were used for verification of AF4-UV-MALS results.

2.5.1. Batch-mode DLS analysis

DLS measurements were performed at a temperature of 25 °C. The dispersion media being water, the solvent refractive index used was 1.331 and viscosity 0.8885 cP. Particle refractive properties used for the conversion to number-based distribution through Mie Scattering model, were those of polystyrene with 1.59 for real part and 0.01 for imaginary part. These values were selected as a compromise due to the polymeric nature of the NPs. For DLS measurements, one drop of sample was deposited onto the sample cell as a suspension, and was irradiated by a laser. The autocorrelation function (ACF) of the scattered light intensity corresponded to the average of 10 consecutive acquisitions of 60 s each. The number of channels and the time intervals were adjusted to 400 and 10 μs, respectively. The laser power was adjusted daily. Each acquisition was processed using the Cumulant algorithm, assuming a monomodal and Gaussian distribution according to the ISO standard [22]. From this model, scattering intensity weighted raw data allowed the determination of the hydrodynamic diameter (Z-average) of the particles and size distribution properties (polydispersity index PDI $=\left(\frac{\text{width}}{\text{Z-average}}\right)^2$, D10, D50, D90 and Span= $\frac{D90-D10}{D50}$).

Mean number size calculated from the same model (Dn_DLS) was also reported for comparison with AF4-MALS data. Method accuracy and daily quality control of DLS measurements were evaluated by the analysis of a certified reference material of polystyrene nanospheres suspension (PS100) prepared in NaCl 10 mM at a concentration of 70 mg(solid)/mL.

2.5.2. AF4-UV-MALS analysis

AF4 separation was performed with a channel including a spacer of 350 μm. Three membranes were used: a regenerated cellulose (RC) with a 5 kDa cut-off, another RC with a 10 kDa cut-off and a 5 kDa polyethersulfone (PES). Sample injection volumes ranging from 20 to 100 μL were studied. Three different mobile phases were also tested (ultrapure water, NaCl 0.1 M and SDS 0.1% w/v). The AF4 elution program applied is summarized in Fig. 2.

The MALS detector allows an absolute determination of particle size based on the angular dependence of the light scattered. The particle size is defined by the gyration radius (Rg), also called root mean square radius, corresponding to the slope of Debye plot using Berry formalism order 2 for detectors located at 44° to 134°. This model was retained based on conclusions of Anderson et al. [39] that concluded this is the most general procedure when the polymer structure or the size are not known. This is also the more appropriate method for large material. In the reported results, the radius value was converted into diameter (Dg = 2 x Rg) for an easier comparison with other techniques. From this diameter, the number average diameter (Dn) and cumulative number fractions (Dn10, Dn50 and Dn90) indicating the size distribution of particles, were calculated using the Astra software. The geometric diameter (Dgeo) derived from the sphere formalism was also obtained.

For NPs shape study, the cross flow gradient was replaced by a constant cross flow of 1 mL/min for 110 min in order to achieve a linear calibration with PS nanospheres, and then extrapolated to the nanoformulations. Based on the diffusion of particles into the AF4 channel, retention times were then converted into hydrodynamic diameter (Dh) across the peak of NPs population. Calibration was performed by injecting a mixture of PS with a concentration of approximately 600, 400, 80 and 40 μg/g in water for PS20, PS50, PS100 and PS200, respectively. The PS suspension prepared for calibration was also used as a quality control sample for AF4 fractionation and MALS particle size calculation.

2.5.3. Additional techniques

2.5.3.1. Electron microscopy analysis. Reconstituted freeze-dried NPs (batch L7) were diluted 10^3 times with ultrapure water and then mixed with the same volume of phosphotungstic acid (2% in water). 1 μL of this solution was then placed on a copper grid (CF400-CU, Electron Microscopy Sciences, USA) and allowed to dry at room temperature. Later, the grid was washed with 1 mL of

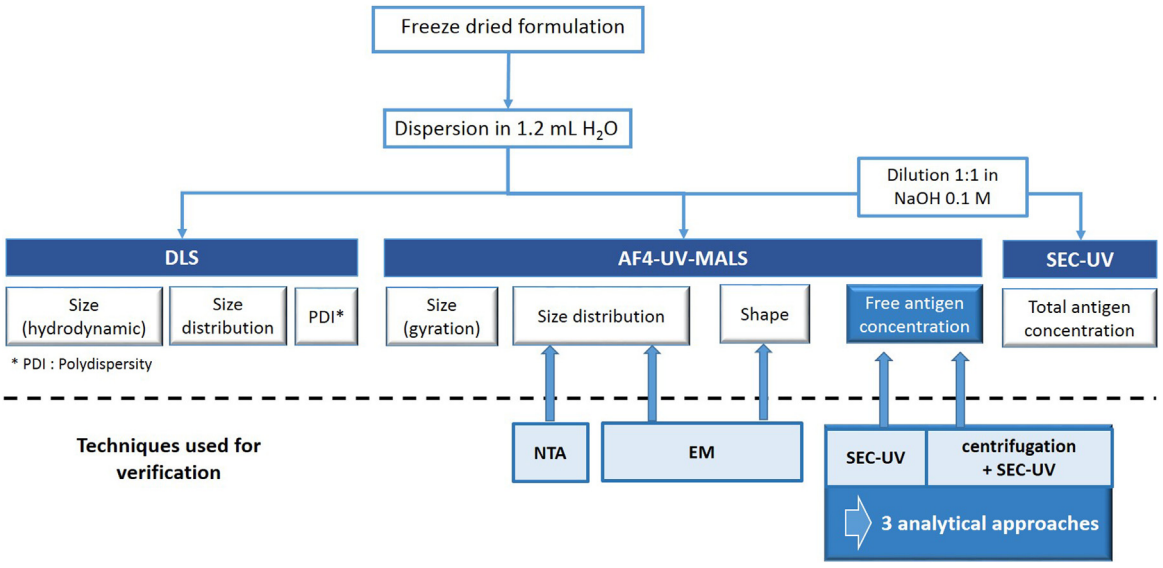

Fig. 1. Analytical procedures applied to the loaded nanoformulation.

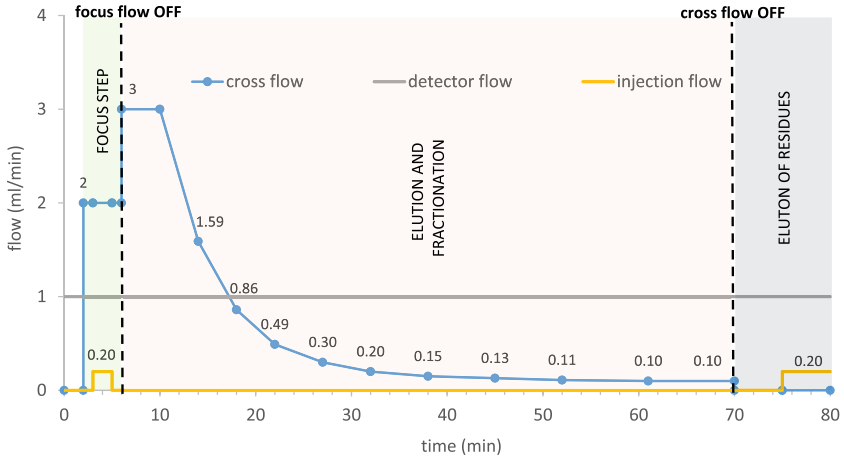

Fig. 2. AF4 elution program.

water and, once dried, analyzed by FESEM. For image treatment, five images were compiled and a total of 169 particles were considered.

2.5.3.2. Nanoparticle tracking analysis. Reconstituted freeze-dried NPs were diluted 10^3 times in ultrapure water prior to analysis. The settings for the shutter and the camera gain were set at 890 and 11, respectively. For each sample, 5 measurements of 60 s each were generated and averaged. Particle concentration distribution is the average of three batches of control formulations (C2 to C4) or loaded formulations (L7 to L9), separately analyzed.

2.5.4. Study of the peptide antigen

Total antigen recovery was first calculated to ensure no drug loss or degradation during formulation process occurred. In most cases, the determination of total drug content is based on its complete release by NPs disruption, followed by the drug specific analysis [40]. In this study, chitosan-dextran sulfate particles were destroyed by dilution of the formulation (1:1) in NaOH 0.1 M as described by Pechenkin et al. [41] and antigen quantification was performed by SEC-UV (Fig. 1). Peptide elution was achieved with phosphate buffer 50 mM ($NaH_2PO_4^-/Na_2HPO_4^{2-}$) and sodium chloride 150 mM with a flow rate of 0.7 mL/min for 35 min. A sample volume of 50 µL was injected. Calibration was obtained with peptide concentrations ranging from 10 to 100 mg/L (6 concentration levels) prepared in NaOH 0.1 M. Total antigen recovery was calculated as the ratio between the antigen concentration determined by SEC-UV and the theoretical total antigen concentration.

The determination of the amount of not associated antigen with NPs, also called free antigen, was carried out by three different analytical approaches (Fig. 1). Two of them (AF4 and SEC, both associated with the UV–vis detector) were performed by direct analysis of the reconstituted nanoformulation. AF4 analysis was performed using conditions optimized for NPs analysis (Fig. 2). For SEC, the same analytical conditions as those used for total antigen recovery analysis were applied. Calibration was performed with peptide concentrations ranging from 20 to 150 mg/L prepared in ultrapure water. The third analytical procedure was based on the separation of the free antigen from NPs by isolating the NPs on a glycerol bed (1% of the formulation) and centrifuging for 2 h at 4 °C with a rotary speed of 16,000 g. Then, the supernatant containing the free antigen was analyzed by SEC-UV with the same analytical conditions than those used for direct analysis.

For each analytical procedure, the free antigen recovery was calculated as the ratio between the amount of free antigen experimentally determined and the theoretical total content.

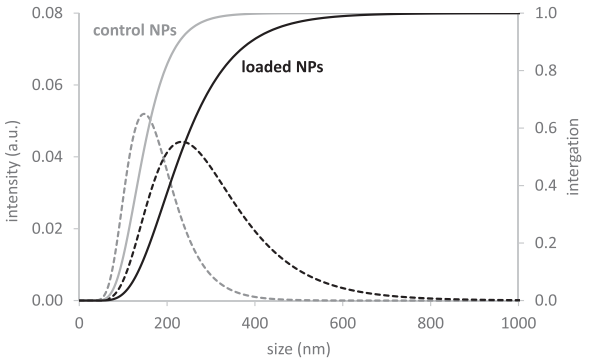

Fig. 3. Comparison of control (grey line) and loaded nanoformulations (black line) signal using batch-mode DLS.

3. Results and discussion

Nanovaccine formulation was composed by chitosan/dextran NPs with the peptide antigen entrapped by ionic interactions. Dextran sulfate was in excess in the formulation to efficiently complex the peptide (positively charged). Several batches were produced in the pilot plant (batches L1 to L9) on different days and then analyzed to evaluate the reproducibility of the process. Control formulations without antigen loading (batches C1 to C4) were also made to better understand interactions between peptide and NPs. Analytical development and performance studies of DLS and AF4 methods were carried out with the loaded formulations since they were the most complex systems.

3.1. Size characterization by batch-mode DLS

The different batches of nanoformulation were first analyzed by DLS to determine if they met the defined size and size distribution specifications (Table 2). Fig. 3 represents the scattered intensity obtained using the cumulant method as well as the cumulative distribution curve. For both formulations, particles in the DLS size range were detected. Relatively low polydispersity values, between 0.1 and 0.2, were obtained with a moderate fluctuation of the residue analysis that did not exceed ± 0.01. Therefore, as described in the ISO reference [22], the cumulant model assuming a monomodal and gaussian distribution seems appropriate.

Several parameters and analytical performances of DLS were then studied in order to ensure a reliable analytical method. Briefly, method specificity was first verified by measuring the absorbance of particles around the laser wavelength (658 nm) to be sure that the light scattering was not altered. The absence of signal showed DLS is specific enough for this application. Signal stability during data acquisition was also verified. A variation of the scattered light intensity lower than 5% and no significant variation of the autocorrelation curve function confirmed satisfactory signal stability during measurements. The working concentration previously defined during formulation development for administration (6.4 wt%) was within both the method linearity range (with R^2 > 0.991 for NPs concentrations ranging from 2 wt% to 8.4 wt%) and the recommended range of scattered light intensity. These working conditions can thus be considered as appropriate. Method accuracy was estimated using the PS100 certified reference material (n = 5). An absolute bias of 3.5 and an expanded uncertainty of 4.3 were obtained for particle size showing a good agreement between the found and certified values. Method precision (repeatability and intermediate precision) was then evaluated considering the batch L2. Results obtained for several parameters (Z-average, PDI, D10, D50, D90 and span) are presented in Table 1. As no criteria were available in the ISO standard for slightly polydisperse NPs, performance thresholds were estimated based on our previous experience with a reasonable approach. During method accuracy determination, a high variation of PDI was observed for the monodisperse PS100 certified reference material (56%) as already reported by Varenne et al. [19]. Thus, the threshold for PDI was set to 50%. Since D10 and D50 are less affected by the presence of a small amount of big particles than D90, the RSD threshold was set at 10% and 20% for these two parameters, respectively. RSD values obtained for repeatability and intermediate precision (Table 1) were all lower than the defined thresholds showing the method was precise enough for the control of produced NPs.

After validation, the DLS method was applied to the analysis of five batches of loaded and not loaded (control batch without antigen) NPs for process variability evaluation. Results are presented in Table 2. Particle size results clearly showed the presence of larger particles in the formulation containing the antigen. This was previously observed in Fig. 3 with hydrodynamic diameters distributed from 60 nm to 800 nm for loaded particles whereas particles from 50 nm to 400 nm were detected for control formulation. On the other hand, size distribution results (Table 2 and Fig. 3) obtained for the loaded formulation indicated that particles ranging from 60 nm to 400 nm represent more than 90% of the NPs population in intensity average.

For all batches of loaded NPs, the values for the different studied parameters complied with the product specifications. Satisfactory batch-to-batch variability was obtained with RSD ranging from 4 to 9% for size dispersion parameters, 21% for PDI and only 3% for Z-average size. Whether they were loaded or not, particles with relatively low polydispersity index (PDI < 0.2) and good reproducibility were manufactured.

DLS thus appeared as a valuable routine technique to control the size of NPs at the production plant. However, it is well-known that its low resolution can hide a more complex particle size composition and may lead to a misleading interpretation as observed by Hansen et al. [42]. Furthermore, Kato et al. [43] demonstrated that the size distribution of particles determined by DLS is rather qualitative and less reliable than those obtained by separative techniques such as AF4. In this study, the significant difference observed Table 2 for intensity (Z-average) and number average diameters (Dn_DLS) for both types of NPs suggested the presence of a considerable amount of small particles shifting the mean size towards lower values. It therefore seems that, despite a relatively low polydispersity (< 0.2), the cumulant model assuming a Gaussian distribution was not perfectly adapted.

3.2. Size characterization by AF4-UV-MALS

Despite its advantages, the information obtained by DLS is rather limited and needs to be confirmed by other techniques as already reported in several studies [14,43]. In this context, an analytical method based on AF4 fractionation was developed. On-line associated with light scattering (MALS) and a concentration detector (UV), AF4 was expected to increase the level of knowledge on the physicochemical properties of the formulation and improve the size resolution.

Different parameters were considered for the optimization of the AF4 fractionation such as mobile phase composition, membrane material and flow rates in order to obtain a good separation of the sample components without significant losses of material during analysis.

3.2.1. Optimization of the AF4 conditions

To obtain a screening of particles over a large size range, the gradient elution presented in Fig. 2 was first applied with a RC10 kDa membrane. No light scattering (LS) signal was detected with ultrapure water or saline solution (NaCl 0.1 M) as mobile phases. For

Table 1
Precision of the DLS method applied to loaded nanoformulation (batch L2).

		Z-average	*D10*	*D50*	*D90*	*Span*	*PDI*	*Dn_DLS (nm)*
Repeatability (RSD)	N* = 10 (same aliquot)	2%	3%	4%	10%	17%	28%	8%
Threshold		5%	10%	10%	20%	ND***1***	50%	ND***1***
Interprecision (RSD)	3 aliquots analyzed on	2%	2%	3%	4%	4%	9%	1%
Threshold	3 different days (N* = 2)	5%	10%	10%	20%	ND***1***	50%	ND***1***

*N: number of replicates.
*1 ND: Not defined.

Table 2
DLS results obtained for batch-to-batch variability study of loaded formulations and comparison with the control formulation.

	Z-average (nm)	PDI	D10 (nm)	D50 (nm)	D90 (nm)	Span	Dn_DLS (nm)
CONTROL NPs							
batch C1 (n*1 = 2)	126 ± 6	0.12 ± 0.03	97 ± 4	151 ± 6	233 ± 13	0.90 ± 0.08	82 ± 9
LOADED NPs							
Specifications (loaded NPs)	***100 - 300***	***< 0.3***	***80 - 150***	***150 - 250***	***250 - 450***	***0.4 - 3***	***ND****
batch L2 (n*1 = 2)	188 ± 3	0.11 ± 0.01	146 ± 3	220 ± 6	329 ± 12	0.83 ± 0.03	139 ± 2
batch L3 (n*1 = 2)	186 ± 10	0.20 ± 0.03	142 ± 8	245 ± 23	419 ± 51	1.12 ± 0.07	105 ± 1
batch L4 (n*1 = 2)	176 ± 6	0.17 ± 0.02	133 ± 4	221 ± 13	368 ± 35	1.06 ± 0.09	103 ± 5
batch L5 (n*1 = 2)	174 ± 1	0.17 ± 0.01	133 ± 4	221 ± 6	371 ± 8	1.08 ± 0.05	101 ± 3
batch L6 (n*1 = 3)	184 ± 10	0.18 ± 0.01	140 ± 7	239 ± 16	397 ± 27	1.08 ± 0.01	108 ± 9
average ± standard deviation	**181 ± 6**	**0.17 ± 0.04**	**139 ± 6**	**229 ± 12**	**377 ± 34**	**1.03 ± 0.12**	**111 ± 16**
RSD interbatches	3%	**2**1%	4%	5%	9%	**1**1%	**1**4%

*ND: Not defined.
*1 duplicate analysis of n aliquots.

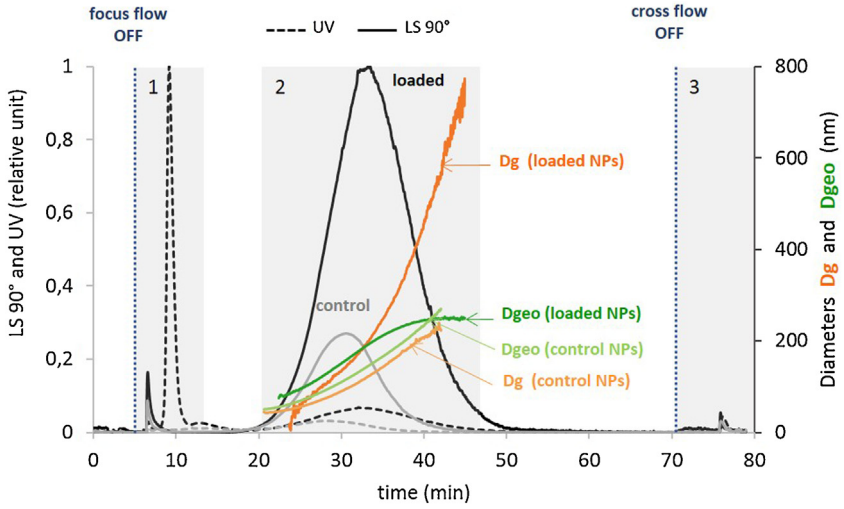

Fig. 4. AF4–UV (dotted line)–MALS (solid line) fractogram obtained for loaded (in black) and control (in grey) formulations in the optimized conditions (Vinj =50 µL; membrane RC 10 kD; mobile phase SDS 0.1% w/v). Calculated gyration diameters Dg (orange lines) and geometric diameters Dgeo (green lines) are also given. (For interpretation of the references to colour in this figure legend, the reader is referred to the web version of this article.)

ultrapure water, this could be explained by the interactions of NPs with the membrane. These interactions were commonly reported in literature for different biomacromolecules and bioparticles such as proteins [44] or liposomes [45]. A review concluded it is not always easy to predict and explain sample-membrane interactions as they mainly depend on the properties of both membrane and mobile phase as well as the characteristics of the sample components [46]. In the case of the saline mobile phase, since NPs are prepared by electrostatic interactions between the forming polymers, the salts present in this carrier are expected to cause their disruption. Finally, the addition of an anionic surfactant to the mobile phase showed to be sufficient to prevent interactions with the membrane without disrupting the particles integrity. A representative AF4-UV-MALS fractogram obtained with 0.1% (w/v) sodium dodecyl sulfate (SDS) as a carrier is presented in Fig. 4. This SDS concentration was adjusted to half of the critical micellar concentration to prevent SDS micelle formation that could disturb MALS measurement [47,48]. Fig. 4 shows satisfactory separation of the different sample components with the elution of particles in an acceptable analysis time. Three different areas can be distinguished. The first area (Fig. 4) revealed the presence of two distinct peaks at 6 and 9 min. The peak at 6 min corresponded to the void volume where small compounds such as the excess of dextran sulfate were eluted, the contribution from the change in the pressure of the AF4 system also observed in the blank (mobile phase) being negligible. The compound eluting at 9 min showed a UV signal but no LS signal. This peak probably corresponded to the antigen since no peak was present when monitoring the UV signal of the control formulation. Injection of the antigen alone was performed and showed a similar retention time with the UV detector. However, with a molecular weight of 2.28 kDa, the antigen is supposed to pass through the ultrafiltration membrane. Thus, a complex based on electrostatic interactions between the amine groups of the antigen and the SDS sulfate group might be formed. A similar observation was made by

Roussel et al. detecting the formation of micelles in the presence of SDS (0.1% w/v), where single SDS molecules bind to a peptide [49]. Therefore, the use of SDS as carrier allowed not only the elution of NPs but also the retention of the peptide on the upper part of the membrane and thus its separation from the particles. The quantification of the peptide in the formulation is further studied in Section 2.4.2.

In the second area of the fractogram (Fig. 4), the LS signal showed the presence of one single broad peak (tr = 34 min) corresponding to the NPs population. The monomodal size distribution assumed by DLS is then in agreement with the AF4 results. At the NPs elution time, a UV signal proportional to NPs concentrations (R^2 > 0.998 from 20 to 100 µL injected volumes) was also obtained. In accordance with the AF4 theory, the radius curve of NPs population increased with elution time. Moreover, the LS signal linearly increased with the injected NPs amount (R^2 > 0.999 from 20 to 100 µL injected volumes) and no significant variation was observed on the retention time (< 5%) demonstrating the absence of overloading. A sample injection volume of 50 µL appeared to be the best compromise to allow complete relaxation of particles with a good signal-to-noise ratio.

Finally, the decrease of LS signal to baseline before the end of the cross flow and the negligible amount detected when cross flow was stopped (third area, Fig. 4) suggested the sample was totally eluted from the channel and negligible amount of aggregates were present.

Afterwards, three membranes with different nature and pore size cut-off were tested: regenerated cellulose with 5 kDa and 10 kDa cut off and polyethersulfone (PES) with 10 kDa cut off. The use of the PES membrane resulted in smaller LS peak area, especially for the first two injections, suggesting interactions with the membrane, not observed with RC membranes. In literature, a significant loss of recovery was also observed when using PES instead of RC membrane for proteins [50] and virus like particles analysis [51].

Size results obtained for loaded NPs were defined as described in the next section and presented for each tested membrane in Fig. 5. An average diameter of 160 ± 10 nm was obtained with all membranes. Size distribution data showed similar particle behavior with both RC membranes whereas a loss of smaller and larger NPs was observed with PES. These results are in agreement with the interactions previously observed for the PES membrane. Moreover, the peptide / SDS complex was more retained and separated from the void volume with the RC membranes than with the PES one. RC 10 kDa membrane was thus selected for this study.

3.2.2. Optimization of the AF4-UV-MALS data treatment

In parallel to the AF4 fractionation optimization, MALS data treatment was studied to ensure accurate size measurement. Gyration (Dg) and geometric (Dgeo) diameters obtained across the peak of NPs by different fitting methods (Berry and sphere formalism, respectively) are shown in Fig. 4. Regarding the loaded NPs, Dg and Dgeo values were similar in the first part of the peak but an increasing divergence in Dg and Dgeo values could be observed beyond 180 nm. In fact, the sphere model fit decreased from R^2 = 0.990 at the peak apex to R^2 = 0.780 at the end of the peak. Due to this size underestimation, the sphere model appeared as not adequate for the measurement of the largest particles. This demonstrates a change in the mass distribution inside the particles and/or in the shape of the particles away from a perfect sphere. With a R^2 > 0.998 over the whole peak, the Berry second order fit without any assumption on particle shape was more appropriate to determine the particles gyration size. Using this model, Dg was distributed from 60 to 700 nm for the loaded formulation (Fig. 4).

Particle size distribution is also an important parameter to control vaccine efficacy. The number-based size distribution calculated from the Berry model with UV used as concentration detector was reported in Fig. 6 as a differential number fraction for an easier comparison of both formulations and also as a cumulative distribution for the determination of Dn10, Dn50 and Dn90 to evaluate the analytical performances and process variability presented Table 3.

Size distribution profiles of both formulations with AF4-UV-MALS (Fig. 6a) were similar to those obtained by NTA (Fig. 6b), indicating that most of loaded NPs (> 90%) had a diameter in the range of 60–250 nm. These results demonstrated the potential of AF4 to determine the number size distribution profile. Otherwise, those results were in agreement with the DLS distribution results (Table 2) that indicated a D90 value of 377 nm. This value is slightly larger as it is related to the intensity-size average of the particles.

Electron microscopy images of loaded NPs are presented in Fig. 7. Data treatment (Fig. 7c) showed particle distribution in the diameter range 50–330 nm with most of the particles (> 90%) ranging from 50 to 270 nm. These values were in accordance with the AF4-MALS and NTA results. Particles above 330 nm were not visualized probably because of the insufficient number of particles which was not representative of the whole sample. It could also be possible that larger particles have been destroyed during the EM sample preparation procedure due to the drying process or by exposition to dyes, vacuum and electron beam as already observed [52].

3.2.3. AF4 analytical performances

Once developed, analytical performances of the AF4 method were assessed. Method repeatability was evaluated by consecutive analysis (n = 6) of the same aliquot of loaded NPs (Table 3). A relative standard deviation lower than 5% was obtained for size parameters. Intermediate precision, determined over three different days of analysis, showed a variability of 10–15% for all size parameters. The AF4 method then appears as precise in repeatable and intermediate precision conditions.

3.2.4. Nanoformulations AF4 analysis

Gyration diameter (Dg) according to the elution time as well as LS fractograms of both control and loaded NPs were compared (Fig. 4). Loaded NPs eluted later than control NPs, indicating the presence of particles with larger hydrodynamic diameters when the antigen was present. A broader size distribution was observed for loaded NPs with Dg from 60 nm to 700 nm whereas Dg from 50 nm to 240 nm was detected for the unloaded control NPs. These results were consistent with those obtained with DLS (Fig. 3). These two methods also gave similar number average sizes (Dn) for both formulations (Tables 2 and 3). Regarding the number size distribution, most particles (> 90%) had a Dg ranging from 40 nm to 120 nm and from 60 nm to 250 nm for control and loaded nanoformulations, respectively (Fig. 6a and Table 3) indicating a low polydispersity as already observed by DLS (PDI < 0.2). Results clearly showed that the presence of antigen in the formulation caused a decrease in the proportion of small particles (40–100 nm) and the formation of larger particles (100–400 nm) (Fig. 6a), which is in agreement with the NTA analysis (Fig. 6b).

The batch-to-batch variability of loaded formulations determined from 5 different batches was lower than 15% for all size distribution parameters (Table 3). Consequently, AF4 results were in accordance with those of DLS indicating that highly reproducible nanoformulations were produced.

3.3. Nanoparticles shape determination

Besides its advantage to accurately determine the size distribution, AF4 is also useful to evaluate the NPs shape by calculating the shape factor ρ (ρ = Dg/Dh) [53]. Absolute hydrodynamic radius across the peak can be obtained by DLS online coupled to AF4 [54,55]. This technique being not available in our laboratory, the

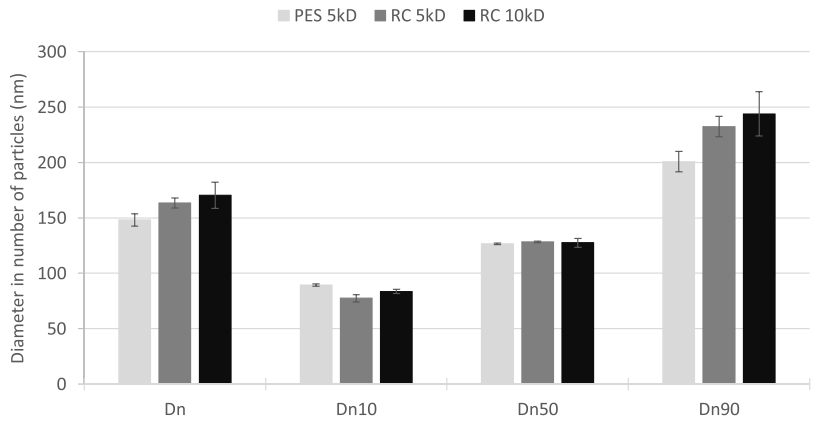

Fig. 5. Average diameter (Dn) and distribution diameters (Dn10, Dn50 and Dn90) obtained by AF4-MALS for loaded formulation with PES 5 kDa (in light grey), RC 5 kDa (in deep grey), and RC 10 kDa (in black) membranes.

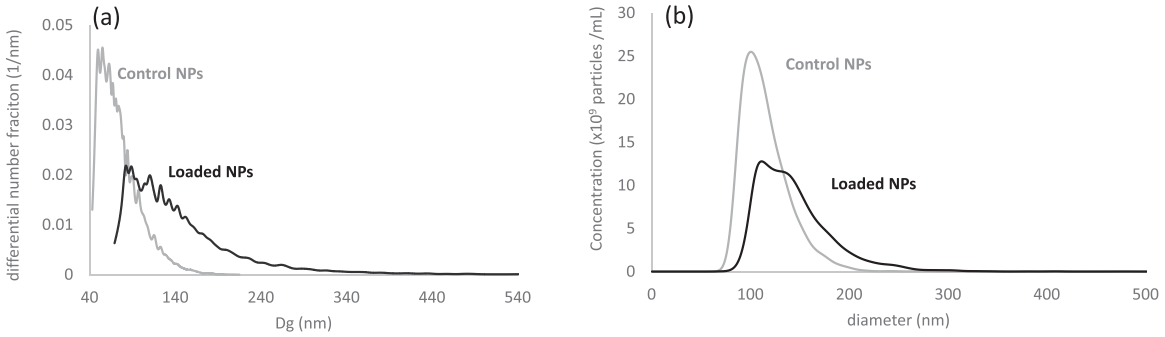

Fig. 6. Number size distribution of loaded (in black) and control (in grey) formulations obtained by (a) AF4-UV-MALS and (b) NTA analysis.

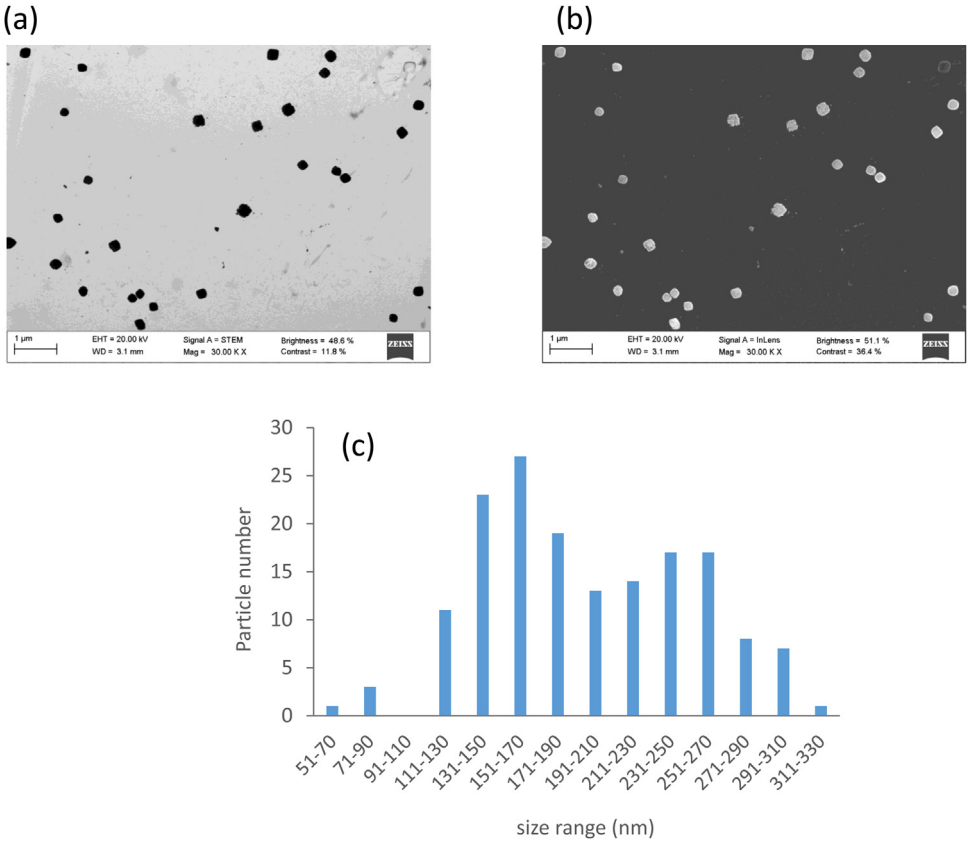

Fig. 7. FESEM imaging of loaded NPs. (a) Image with STEM detector; (b) Image with InLens detector; (c) Size distribution obtained by Image J data treatment.

Table 3
AF4-MALS results obtained for batch-to-batch variability study of loaded formulations and comparison with control formulation. Precision performances were also studied (batch L6).

	Dg (nm)	Dn (nm)	Dn10 (nm)	Dn50 (nm)	Dn90 (nm)
CONTROL NPs					
batch C1 (n* = 3)	127 ± 11	85 ± 6	51 ± 2	73 ± 4	118 ± 10
LOADED NPs					
batch L2 (n* = 2)	398 ± 16	171 ± 12	84 ± 3	131 ± 5	245 ± 21
batch L3 (n* = 2)	456 ± 15	154 ± 15	76 ± 7	130 ± 3	251 ± 16
batch L4 (n* = 2)	365 ± 25	131 ± 9	62 ± 3	109 ± 3	207 ± 11
batch L5 (n* = 2)	327 ± 3	132 ± 2	64 ± 3	106 ± 1	196 ± 3
batch L6 (n* = 3)	364 ± 42	156 ± 16	72 ± 2	117 ± 8	233 ± 29
average ± standard deviation	**382 ± 49**	**149 ± 17**	**72 ± 9**	**119 ± 12**	**226 ± 24**
RSD interbatches	**13%**	**12%**	**13%**	**10%**	**10%**
RSD repeatability	**1.7%**	**1.4%**	**1.7%**	**1.5%**	**1.5%**
RSD interprecision	**11%**	**5%**	**1%**	**6%**	**7%**

*Duplicate analysis of n aliquots.

retention time was converted into hydrodynamic radius with PS calibrants on the basis of the theoretical diffusion of the particles into the AF4 channel. However, several studies have reported that the behavior of NPs inside the AF4 channel can be highly influenced by particle interactions [56–58]. Those interactions are mainly due to the surface charge of particles and can be dependent on the membrane lifetime. Thus, to minimize the deviation that could occur between analytes and standards, the calibration was daily performed and surface charge values were compared. With a zeta potential of -27 ± 2 mV for NPs and -34 ± 3 mV for PS calibrants, similar diffusion behavior into the AF4 channel was assumed, allowing the PS calibrants to be used for hydrodynamic radius determination. In accordance with the AF4 theory, a linear PS calibration curve with $R^2 > 0.998$ was obtained.

The LS signals for control and loaded NPs are shown in Fig. 8. Hydrodynamic diameter (Dh), gyration diameter (Dg) and the calculated shape factor (ρ) are also presented. Considering control NPs (Fig. 8a), a constant $\rho = 0.85 \pm 0.03$ was obtained across the peak. With $0.78 \leq \rho \leq 1$ (0.78 for a homogeneous solid sphere and 1 for an empty sphere [53]), control NPs had a moderately hard spherical structure of non-uniform density. In this case, the sphere model fit was appropriate all over the peak ($R^2 > 0.990$) with Dgeo distributed from 60 to 230 nm, close to Dg values.

Regarding the loaded NPs (Fig. 8b), the Berry model did not fit in the first part of the peak and a very noisy signal at the end impeded an accurate measurement of Dg. These results clearly showed the necessity to use cross flow gradient fractionation for an adequate Dg determination all over the peak. Nevertheless, in the Dg range of 60–400 nm, the increase of ρ across the peak indicated small changes in the NPs structure according to the size. A structural modification of the loaded particles was observed from a soft full sphere ($\rho = 0.8$) to a random coil structure ($\rho = 1.2$–1.3) in correlation with the decrease of the sphere model fit previously observed with cross flow gradient. This slight change of structure away from sphere affected particles above 200 nm, representing less than 15 % of the particle population.

Micrographs of loaded formulation showed particles with a spherical appearance but with irregular edges (Fig. 7a and b). The structural changes revealed by AF4 were not observed by EM. These results demonstrated that AF4 could be a powerful tool to study NPs slight structural changes and nanovaccines as well as size distribution.

3.4. Peptide antigen content in the nanoformulation

3.4.1. Total antigen recovery

Another critical attribute that needs to be assessed for regulatory purposes is the total drug content in the formulation to verify its integrity. To obtain this information, the antigen was released from the particles by adding NaOH in order to disrupt the ionic interactions between the forming polymers [41]. The efficacy of the particle disruption procedure was checked by AF4-MALS and DLS and no particles were detected by both methods. However, the use of NaOH led to a significant and non-reproducible peptide carryover from the AF4 membrane hindering its recovery determination by AF4-UV. SEC-UV was used instead to quantify the total peptide content. The chromatogram showed a well-defined peak at 18.9 min corresponding to the peptide which was proportional to its concentration ($R^2 > 0.995$). Disrupted formulations were previously spiked with peptide antigen at two concentration levels (30 mg/L and 60 mg/L) and recoveries of 105% and 112% were obtained, respectively, indicating no significant matrix effect. The method was then applied to three different batches of loaded particles. Recoveries between 91% and 110% were obtained ensuring no loss of antigen occurred during the manufacturing process.

3.4.2. Free antigen quantification

The free drug in nanoformulations is usually determined by filtration and/or centrifugation to isolate it from NPs prior to its quantification [40]. The limitation of this procedure is that filters or centrifuge tubes might adsorb or alter the analyte and dilution might lead to drug release [16]. To avoid these problems, we developed a rapid AF4-UV method allowing the quantification of the free antigen simultaneously with the determination of the particle size distribution. The antigen was eluted at 9 min in its complexed form with SDS (Fig. 4). A linear calibration curve was obtained ($R^2 > 0.995$) and no retention on the AF4 membrane was observed. However, special attention was paid to the formation of the complex that could be disturbed by formulation components. To evaluate the matrix effect, the formulation was spiked with antigen at 30 mg/L and 60 mg/L and recoveries of 114% and 100% were obtained, respectively. These results showed no matrix effect demonstrating that antigen quantification by external calibration was accurate.

This method was compared to two other analytical strategies (SEC-UV without sample preparation and SEC-UV after centrifugation) and results are presented in Table 4.

No deviation was observed for the three different analytical approaches demonstrating AF4-UV is able to accurately quantify the active ingredient. Similar results obtained with and without sample treatment showed that the centrifugation step did not release the antigen from the particles.

Surprisingly, results in Table 4 indicated that 84% of the antigen was present in the formulation as non-associated with NPs. However, any type of particles separation from their surrounding medium including SEC or AF4 as well as sample dilution into the mobile phase could potentially disturb the concentration equilibrium of the drug between the loaded and the free form. It is

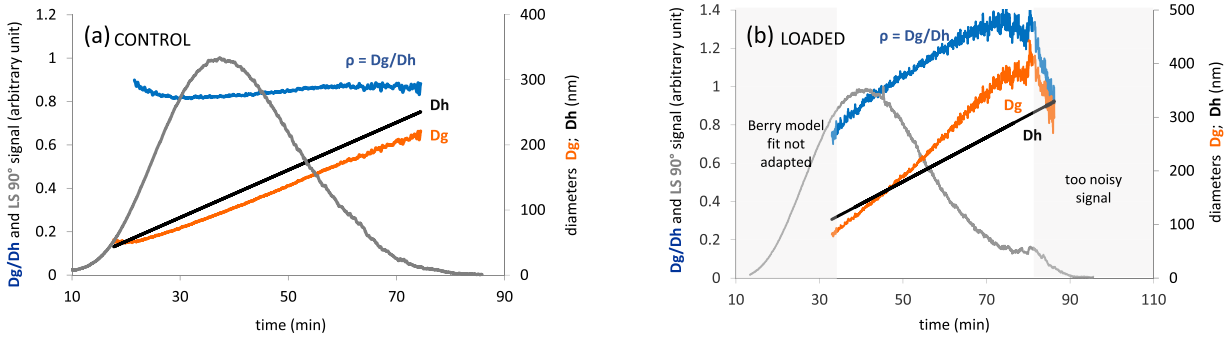

Fig. 8. AF4-MALS fractogram obtained at angle 90° in isocratic elution mode for (a) control NPs and (b) loaded NPs. The calculated gyration diameter Dg (in orange), hydrodynamic diameter Dh (in black) and the ratio Dg/Dh (in blue) are also presented. (For interpretation of the references to colour in this figure legend, the reader is referred to the web version of this article.)

Table 4
Free antigen recoveries of four loaded nanoformulations determined by three different analytical approaches (AF4-UV, SEC-UV and SEC-UV after centrifugation).

Batch number	AF4-UV direct	SEC-UV direct	SEC-UV after centrifugation
batch L1 (n* = 1)	77 ± 3%	80 ± 1%	82 ± 1%
batch L3 (n* = 2)	90 ± 2%	87 ± 2%	86 ± 1%
batch L4 (n* = 2)	84 ± 4%	84 ± 1%	83 ± 1%
batch L6 (n* = 3)	83 ± 4%	85 ± 1%	85 ± 1%
average ± standard deviation	**84 ± 6%**	**84 ± 3%**	**84 ± 2%**
RSD interbatches	**7%**	**4%**	**3%**

*Duplicate analysis of n aliquots.

also possible that part of the non-associated antigen has formed a complex with dextran sulfate with an opposite charge and in excess in the formulation. Since this complex might be very labile, the peptide could be released from dextran sulfate during SEC or AF4 separation. Then, the amount of antigen found as free by the three analytical procedures could correspond to a mixture of free antigen and antigen complexed with dextran sulfate. This could explain the difference observed in a previous study where 80% of antigen was found associated with the NPs fraction using preparative SEC [38]. This fraction probably corresponded to the mixture of antigen complexed with dextran and antigen associated with NPs.

4. Conclusion and perspectives

The combined use of DLS and AF4 techniques showed that the studied polymeric NPs were manufactured with a high degree of uniformity and interbatch reproducibility. The batch-to-batch variability was lower than 16% for size and size distribution of loaded NPs and the polydispersity index ranged from 0.1 to 0.2. In that case, DLS was shown to be a valuable routine technique to control the NPs size. However, the assumption of a monomodal distribution of spherical particles had to be verified. As a complementary technique, AF4 coupled to UV–vis and LS detectors provided, in one single analytical run, the following parameters for the rigorous characterization of the nanoformulation: quantification of free antigen (UV), gyration size, size distribution, shape and shape modifications across the size (MALS).

To our knowledge, this is the first time that analytical performances of AF4 have been reported for a nanopharmaceutical and this study showed its high potential for this type of formulation. AF4-UV-MALS showed a variability lower than 5% and 15% for size and size distribution results in repeatable and intermediate precision conditions, respectively. Thus, this technique appears as a robust and powerful analytical tool for the quality control of NPs and for monitoring sample stability. Therefore, it can be applied not only at the early stage of pharmaceutical development but also for regulatory acceptance.

A significant difference was observed for control and loaded NPs in terms of size and particle concentration. The presence of antigen resulted in the formation of larger particles, a decrease in the amount of small particles and a change of shape from spherical to random coil structure.

Acknowledgments

The authors gratefully acknowledge Lucile Marigliano for zetapotential measurements at the IPREM institute (University of Pau, France).

Funding

This work was carried out in the frame of the Nanopilot project funded from the European Union Framework Programme for Research and Innovation HORIZON 2020 under Grant Agreement 646142.

References

[1] H.K.S. Yadav, M. Dibi, A. Mohammad, A.E. Srouji, Nanovaccines formulation and applications – a review, J. Drug Deliv. Sci. Technol. 44 (2018) 380–387.
[2] T.G. Dacoba, A. Olivera, D. Torres, J. Crecente-Campo, M.J. Alonso, Modulating the immune system through nanotechnology, Semin. Immunol. 34 (2017) 78–102.
[3] K.S. Soppimath, T.M. Aminabhavi, A.R. Kulkarni, W.E. Rudzinski, Biodegradable polymeric nanoparticles as drug delivery devices, J. Control. Release 70 (2001) 1–20.
[4] A. Hajizade, F. Ebrahimi, A.-H. Salmanian, A. Arpanaei, J. Amani, Nanoparticles in vaccine development, J Applied Biotech Reports. 1 (4) (2014) 125–134.
[5] B. Bernocchi, R. Carpentier, D. Betbeder, Nasal nanovaccines, Int. J. Pharm. 530 (2017) 128–138.
[6] P. Calvo, C. Remunan-Lopez, J.L. Vila-Jato, M.J. Alonso, Novel hydrophilic chitosan and chitosan / polyethylene oxide nanoparticles as protein carriers, J. Appl. Polym. Sci. 63 (1997) 125–132.
[7] R. Fernandez-Urrusuno, P. Calvo, C. Remunan-Lopez, J.L. Vila-Jato, M.J. Alonso, Enhancement of nasal absorption of insulin using chitosan nanoparticles, Pharm. Res. 16 (1999) 1576–1591.
[8] V. Agarwal, M. Bajpai, A. Sharma, Patented and approval scenario of Nanopharmaceuticals with relevancy to biomedical application, manufacturing procedure and safety aspects, Recent Pat. Drug Deliv. Formul. 12 (2018) 40–52.

[9] S. Bremer, B. Halamoda-Kenzaoui, S.E. Borgos, Identification of regulatory needs for nanomedicines, in: JRC Technical Reports, 2016.
[10] R. Pita, F. Ehmann, M. Papaluca, Nanomedicines in the EU – regulatory overview, AAPS J. 18 (6) (2016) 1576–1582.
[11] M. Elsabahy, K.L. Wooley, Design of polymeric nanoparticles for biomedical delivery applications, Chem. Soc. Rev. 41 (2012) 2545–2561.
[12] N. Benne, J. Van Duijn, J. Kuiper, W. Jiskoot, B. Slütter, Orchestrating immune responses: how size, shape and rigidity affect the immunogenicity of particulate vaccines, J. Control. Release 234 (2016) 124–134.
[13] M. Gaumet, A. Vargas, R. Gurny, F. Delie, Nanoparticles for drug delivery: the need for precision in reporting particle size parameters, Eur. J. Pharm. Biopharm. 69 (2008) 1–9.
[14] F. Varenne, A. Makky, M. Gaucher-Delmas, F. Violleau, C. Vauthier, Multimodal dispersion of nanoparticles: a comprehensive evaluation of size distribution with 9 size measurement methods, Pharm. Res. 33 (2016) 1220–1234.
[15] F. Caputo, J. Clogston, L. Calzolai, M. Rosslein, A. Prina-Mello, Measuring particle size distribution of nanoparticle enabled medicinal products, the joint view of EUNCL and NCI-NCL. A step by step approach combining orthogonal measurements with increasing complexity, J. Control. Release 299 (2019) 31–43.
[16] S. Gioria, F. Caputo, P. Urban, C.M. Maguire, S. Bremer-Hoffmann, A. Prina-Mello, L. Calzolai, D. Mehn, Are existing standards methods suitable for the evaluation of nanomedicines: some case studies, Nanomed. 13 (5) (2018) 539–554.
[17] B. Halamoda-Kenzaoui, U. Holzwarth, G. Roebben, A. Bogni, Bremer Hoffmann S. Mapping of the available standards against the regulatory needs for nanomedicines WIREs, Nanomed. Nanobiotechnol. 11 (2019) e153.
[18] S. Peretz Damari, D. Shamrakov, M. Varenik, E. Koren, E. Nativ-Roth, Y. Barenholz, O. Regev, Practical aspects in size and morphology characterization of drug-loaded nano-liposomes, Int. J. Pharm. 547 (2018) 648–655.
[19] F. Varenne, J. Botton, C. Merlet, M. Beck-Broichsitter, F.X. Legrand, C. Vauthier, Standardization and validation of a protocol of size measurements by dynamic light scattering for monodispersed stable nanomaterial characterization, Colloids Surf. A: Physicochem. Eng. Aspects. 486 (2015) 124–138.
[20] H. Kato, A. Nakamura, M. Shimizu, H. Banno, Y. Kezuk, K. Matsubara, K. Hosoi, S. Yoshida, T. Fujimoto, Acceleration of dispersing calcium carbonate particle in aqueous media using jet milling method, Colloids Surf. A: Physicochem. Eng. Aspects. 520 (2017) 570–579.
[21] T. Zheng, S. Bott, Q. Huo, Techniques for accurate sizing of gold nanoparticles using dynamic light scattering with particular application to chemical and biological sensing based on aggregate formation, ACS Appl. Mater. Interfaces 8 (33) (2016) 21585–21594.
[22] ISO 22412, Particle Size Analysis- Dynamic Light Scattering (DLS), 2017.
[23] G. Brusotti, E. Calleri, R. Colombo, G. Massolini, F. Rinaldi, C. Temporini, Advances on size exclusion chromatography and applications on the analysis of protein biopharmaceuticals and protein aggregates: a mini review, Chromatographia. 81 (2018) 3–23.
[24] Z. Wei, M. McEvoy, V. Razinkov, A. Polozka, E. Li, J. Casas-Finet, G.I. Tous, P. Balu, A.A. Pan, H. Mehta, M.A. Schenerman, Biophysical characterization of influenza virus subpopulations using field flow fractionation and multiangle light scattering: Correlation of particle counts, size distribution and infectivity, J. Virol. Methods 144 (2007) 122–132.
[25] S. Süß, C. Metzger, C. Damm, D. Segets, W. Peukert, Quantitative evaluation of nanoparticle classification by size-exclusion chromatography, Powder Technol. 339 (2018) 264–272.
[26] A. Zattoni, B. Roda, F. Borghi, V. Marassi, P. Reschiglian, Flow Field Flow Fractionation for the analysis of nanoparticles used in drug delivery, J. Pharm. Biomed. Anal. 87 (2014) 53–61.
[27] M.I. Malik, H. Pasch, Field-flow fractionation : new and exciting perspectives in polymer analysis, Prog. Polym. Sci. 63 (2016) 42–85.
[28] M. Wagner, S. Holzschuh, A. Traeger, A. Fahr, U.S. Schubert, Asymmetric flow field-flow fractionation in the field of nanomedicine, Anal. Chem. 86 (2014) 5201–5210.
[29] W. Fraunhofer, G. Winter, The use of asymmetrical flow field-flow fractionation in pharmaceutics and biopharmaceutics, Eur. J. Pharm. Biopharm. 58 (2004) 369–383.
[30] B. Roda, A. Zattonia, P. Reschiglian, M. Hee Moon, M. Mirasoli, E. Michelini, A. Roda, Field-flow fractionation in bioanalysis: a review of recent trends, Anal. Chim. Acta 635 (2009) 132–143.
[31] ISO 21362, Nanotechnologies — Analysis of Nano-objects Using Asymmetrical-flow and Centrifugal Field-flow Fractionation, 2018.
[32] M. McEvoy, V. Razinkov, Z. Wei, J.R. Casas-Finet, G.I. Tous, M.A. Schenerman, Improved particle counting and size distribution determination of aggregated virus populations by asymmetric flow field-flow fractionation and multiangle light scattering techniques, Biotechnol. Prog. 27 (2) (2011) 547–554.
[33] T.J. Evjen, S. Hupfeld, S. Barnert, S. Fossheim, R. Schubert, M. Brandl, Physicochemical characterization of liposomes after ultrasound exposure-mechanisms of drug release, J. Pharm. Biomed. Anal. 78 (2013) 118–120.
[34] ICH Q2(R1) Validation of analytical procedures : Text and methodology.
[35] C.A. Schneider, W.S. Rasband, K.W. Eliceiri, NIH Image to ImageJ: 25 years of image analysis, Nat. Methods 9 (7) (2012) 671–675.
[36] Luo M. European Patent Application: 12767885.2-1401 PCT/CA2012050220- Protease cleavage site peptides as an HIV vaccine.
[37] H. Li, M. Nykoluk, L. Li, L.R. Liu, R.W. Omange, G. Soule, L.T. Schroeder, N. Toledo, M.A. Kashem, J.F. Correia-Pinto, B. Liang, N. Schultz-Darken, M.J. Alonso, J.B. Whitney, F.A. Plummer, M. Luo, Natural and cross-inducible Anti-SIV antibodies in mauritian Cynomolgus macaques, PLoS One 12 (10) (2017) 1–20.
[38] T.G. Dacoba, R.W. Omange, H. Li, J. Crecente-Campo, M. Luo, M.J. Alonso, Polysaccharide nanoparticles can efficiently modulate the immune response against an HIV peptide antigen, ACS Nano (2019), in press.
[39] M. Andersson, B. Wittgren, K.G. Wahlund, Accuracy in multiangle light scattering measurements for molar mass and radius estimations, Model Calculations Exp. Anal Chem. 75 (2003) 4279–4291.
[40] A. Gómez-Hens, J.M. Fernández-Romero, Analytical methods for the control of liposomal delivery systems, Trends Analyt. Chem. 25 (2) (2006) 167–178.
[41] M.A. Pechenkin, N.G. Balabushevich, I.N. Zorov, L.K. Staroseltseva, E.V. Mikhalchik, V.A. Izumrudov, N.I. Larionova, Design in vitro and in vivo characterization of chitosan-dextran sulfate microparticles for oral delivery of insulin, ABB. 3 (10) (2011) 244–250.
[42] M. Hansen, M.C. Smith, R.M. Crist, J.D. Clogston, S.E. McNeil, Analyzing the influence of PEG molecular weight on the separation of PEGylated gold nanoparticles by asymmetric-flow field-flow fractionation, Anal. Bioanal. Chem. 407 (2015) 8661–8672.
[43] H. Kato, A. Nakamura, K. Takahashi, S. Kinugasa, Accurate size and size-distribution determination of polystyrene latex nanoparticles in aqueous medium using dynamic light scattering and asymmetrical flow field flow fractionation with multi-angle light scattering, Nanomater. Basel (Basel) 2 (2012) 15–30.
[44] S. Schachermeyer, J. Ashby, M. Kwon, W. Zhong, Impact of carrier fluid composition on recovery of nanoparticles and proteins in flow field flow fractionation, J. Chromatogr. A 1264 (2012) 72–79.
[45] S. Hupfeld, D. Ausbacher, M. Brandl, Asymmetric flow field-flow fractionation of liposomes: 2. Concentration detection and adsorptive loss phenomena, J. Sep. Sci. 32 (2009) 3555–3561.
[46] U.B. Kavurt, M. Marioli, W. Kok, D. Stamatialis, Membranes for separation of biomacromolecules and bioparticles via flow field-flow fractionation, Chem. Technol. Biotechnol. 90 (1) (2015) 11–18.
[47] S. Paillet, B. Grassl, J. Desbrières, Rapid and quantitative determination of critical micelle concentration by automatic continuous mixing and static light scattering, Anal. Chim. Acta 636 (2009) 236–241.
[48] G. Dupuis, J. Rigolini, G. Clisson, D. Rousseau, R. Tabary, B. Grassl, Determination of the macromolecular dimensions of hydrophobically modified polymers by micellar size exclusion chromatography coupled with multiangle light scattering, Anal. Chem. 81 (2009) 8993–9001.
[49] G. Roussel, Y. Caudano, A. Matagne, M.S. Sansom, E.A. Perpète, C. Michaux, Peptide-surfactant interactions: a combined spectroscopic and molecular dynamics simulation approach, Spectroc Acta A 190 (2018) 464–470.
[50] K.H. Kim, M.H. Moon, Chip-type asymmetrical flow field-flow fractionation channel coupled with mass spectrometry for top-down protein identification, Anal. Chem. 83 (2011) 8652–8658.
[51] R. Lang, L. Vogt, A. Zurcher, G. Winter, Asymmetrical flow FFF as an analytical tool for the investigation of the physical stability of virus-like particles, LC GC N. Am. 27 (2009) 844–852.
[52] Y.P. Chuan, Y.Y. Fan, L. Lua, A.P. Middelberg, Quantitative analysis of virus-like particle size and distribution by field-flow fractionation, Biotechnol. Bioeng. 99 (6) (2008) 1425–1433.
[53] A.K. Brewer, A.M. Striegel, Particle size characterization by quadruple-detector hydrodynamic chromatography, Anal. Bioanal. Chem. 393 (2009) 295–302.
[54] J. Gigault, T.M. Nguyen, J.M. Pettibone, V.A. Hackley, Accurate determination of the size distribution for polydisperse, cationic metallic nanomaterials by asymmetric-flow field flow fractionation, J. Nanopart. Res. 16 (2014) 2735–2745.
[55] P.L. Ma, M.D. Buschmann, F.M. Winnik, One-step analysis of DNA/Chitosan complexes by field-flow fractionation reveals particle size and free chitosan content, Biomacromolecules 11 (2010) 549–554.
[56] J. Gigault, V.A. Hackley, Observation of size-independent effects in nanoparticle retention behavior during asymmetric-flow field-flow fractionation, Anal. Bioanal. Chem. 405 (2013) 6251–6258.
[57] S. Schachermeyer, J. Ashby, M. Kwon, W. Zhong, Impact of carrier fluid composition on recovery of nanoparticles and proteins in flow field flow fractionation, J. Chromatogr. A 1264 (2012) 72–79.
[58] I. De la Calle, M. Menta, M. Klein, B. Maxit, F. Séby, Towards routine analysis of TiO2 (nano-)particle size in consumer products: evaluation of potential techniques, Spectroc Acta B. 147 (2018) 28–42.